Acta Oceanol. Sin., 2019, Vol. 38, No. 3, P. 1–16
https://doi.org/10.1007/s13131-019-1361-2
http://www.hyxb.org.cn
E-mail: hyxbe@263.net

Weather induced subtidal flows through multiple inlets of an arctic microtidal lagoon

Chunyan Li[1], Kevin M. Boswell[2], Nazanin Chaichitehrani[3], Wei Huang[1], Renhao Wu[4]*

[1] Department of Oceanography and Coastal Sciences, College of the Coast and Environment, Louisiana State University, Baton Rouge, LA 70803, USA

[2] Department of Biological Sciences, Florida International University, North Miami, FL 33181, USA

[3] Horn Point Laboratory, Center for Environmental Science, University of Maryland, Cambridge, MD 21613, USA

[4] College of Marine Sciences and Technology, Zhejiang Ocean University, Zhoushan 316022, China

Received 10 October 2018; accepted 10 January 2019

Abstract

Estuarine processes in the arctic lagoons are among the least studied but important subjects, especially considering the rapid warming of arctic water which may change the length of ice-free period in the summer. In this paper, wind-driven exchange flows in the micro-tidal Elson Lagoon of northern Alaska with multiple inlets of contrasting widths and depths are studied with *in situ* observations, statistical analysis, numerical experiments, a regression model on the basis of dynamics, and remote sensing data. Water velocity profiles were obtained from a bottom deployed acoustic Doppler current profiler (ADCP) in the northwestern Eluitkak Pass connecting the Beaufort Sea to the Elson Lagoon during a 4.9 day ice-free period in the summer of 2013. The subtidal flow is found correlated with wind (R^2 value ~96%). Frequently occurring east, northeast and north winds from the arctic atmospheric high- and low-pressure systems push water from the Beaufort Sea into the lagoon through the wide inlets on the eastern side of the lagoon, resulting in an outward flow against the wind at the narrow northwestern inlet. The counter-wind flow is a result of an uneven wind forcing acting through the asymmetric inlets and depth, an effect of "torque" or vorticity. Under northwest wind, the exchange flow at the northwestern inlet reverses its direction, with inward flows through the upwind northwestern inlet and outward flows through the downwind eastern inlets. A regression model is established based on the momentum equations and Taylor series expansions. The model is used to predict flows in July and August of 2015 and July of 2017, supported by available Landsat satellite images. About 73%–80% of the time the flows at Eluitkak Pass are out of Elson Lagoon for the summer of 2015 and 2017. Numerical experiments are conducted to corroborate the findings and illustrate the effects under various wind conditions. A quasi-steady state balance between wind force and surface pressure gradient is confirmed.

Key words: wind-driven flows, multiple inlets, micro-tidal, numerical model experiments, counter-wind flows, quasi-steady state

Citation: Li Chunyan, Boswell Kevin M., Chaichitehrani Nazanin, Huang Wei, Wu Renhao. 2019. Weather induced subtidal flows through multiple inlets of an arctic microtidal lagoon. Acta Oceanologica Sinica, 38(3): 1–16, doi: 10.1007/s13131-019-1361-2

1 Introduction

A coastal lagoon or estuarine embayment is often connected to the coastal ocean through multiple tidal inlets (van de Kreeke, 1985a, 1985b, 1990; Aubrey and Giese, 1993; Janzen and Wong, 1998; Pacheco et al., 2010), serving as passages for land-ocean exchange and interactions. The exchange of water between the coastal ocean and these lagoons can be very different from that between coastal ocean and a conventional coastal plain estuary which normally has a single opening. The latter has been the focus of study for more than sixty years (e.g., since Pritchard, 1956). The study on the Eastern Shore Lagoon of the Delmarva Peninsula (Brumbaugh, 1996) is an example showing the difference between a single opening estuary and a multiple inlet lagoon. The study suggests possible dominant inward flows in certain inlets and outward flows in other inlets of the same system. In a shallow and broad estuary with restricted connection to the coastal ocean, such as the "choked" (Kjerfve and Magill, 1989) Calcasieu Lake (Lin et al., 2016) and enclosed systems such as Lake Rotorua in New Zealand (Gibbs et al., 2016), the circulation is mostly wind-driven, influenced by geometry and bathymetry. Wind is found to determine circulations in the multi-inlet Lake Pontchartrain (Li et al., 2009; Haralampides, 2000) of Louisiana, in the Sapelo and Altamaha Sounds in coastal Georgia (Li, 2013), in the multiple inlet western Dutch Wadden Sea (Duran-Matute et al., 2016), in the East Frisian Wadden Sea multiple inlet system (Herring and Winter, 2015), in the ten Mediterranean lagoons (Umgiesser et al., 2014), and in elongated lagoons such as that in the southern Gulf of Mexico (Casares-Salazar et al., 2016).

For systems with multiple inlets, the exchange flows have certain characteristics. Recent studies in Lake Pontchartrain Estuary (Hunag and Li, 2017) and Port Fourchon (Li et al., 2018b), both micro-tidal systems with narrow inlets in southern Louisiana,

Foundation item: The National Key R & D Project of China under contract No. 2017YFC1404201; the USA North Pacific Research Board Project under contract No.1229 and the USA Bureau of Ocean Energy Management Awards under contract Nos M12PG00024 (ACES) and M12PG00018 (Arctic EIS).

*Corresponding author, E-mail: mikewu@zjou.edu.cn

demonstrate that atmospheric cold fronts (Huang and Li, 2017; Li et al., 2019), warm fronts, and combinations of them (Li et al., 2018b) can produce significant wind-driven subtidal circulation and transport. In Huang et al. (2002), a numerical model is used to study the circulation within a bay in Florida which shows complex response due to tidal oscillations interacting with five inlets. A numerical experiment is used (Li, 2013) to determine the impact of wind in a multiple inlet lagoon system, in which it is shown that for along-shore winds, the outward flow usually occurs through the downwind inlet and inward flow through the upwind inlet. For cross shore winds, the wind-driven flow is usually in the downwind direction through the shallower inlet(s) but against the wind in the deepest inlet, given that these inlets have comparable widths. Duran-Matute et al. (2016) find that water volume transport through the multiple-inlet system of Dutch Weddan Sea is mostly determined by wind, and is much more sensitive to two specific directions. Depending on each individual inlet, the sensitivity is measured by a conductance of transport as a function of wind direction.

Because of the wide range of lagoons and infinite number of possibilities in terms of their geometry, number of inlets, orientation, location and geometry of inlets, and associated dynamics, it is necessary to group them by a relatively simple classification. Kjerfve (1986) classifies lagoons into “choked”, “restricted”, and “leaky” categories with 10 examples. The choked lagoons have one narrow channel connecting the coastal ocean, while the leaky lagoons have more connections to the ocean, and the restricted lagoons are those between the choked and leaky ones. The Elson Lagoon being analyzed in this study can be categorized as leaky lagoon due to the accessibility to the open ocean through its multiple inlets. Our study focuses on wind-driven dynamics in this multiple inlet lagoon. We use *in situ* observations, data analysis, numerical experiments, and remote sensing data to achieve this goal.

2 Study area and observations

2.1 *Study site*

The Elson Lagoon (Fig. 1) is the northern most coastal lagoon of the United States bounded roughly by 71°12′N, 71°23′N, 156°36′W, and 155°54′W. It is approximately a rectangle of ~8 km × 25 km (Fig. 1), with shallow water (2–3 m) in the interior and deeper channels at the passes leading to the coastal ocean and Beaufort Sea. The Elson Lagoon is oriented in the northwest-southeast direction. The axis of the lagoon is estimated to have a ~–30° angle from the true west-east direction (Fig. 1b). It is part of a larger lagoon of a flipped “L” (Fig. 1a). Along the coastal side, there is about 11 km open to the ocean between barrier islands. This larger lagoon has a length scale of ~55 km in either direction of the flipped “L” (Fig. 1a). The deepest location is at the northwestern-most channel, the Eluitkak Pass, with a maximum water depth of ~16 m and width of ~275 m. East and southeast of the Eluitkak Pass, there is a chain of islands (i.e., the Crescent, Tapkaluk, and Cooper Islands). The width of the inlet between Crescent Island and Tapkaluk Island is ~0.7 km, while that between Tapkaluk Island and Cooper Island (the Ekilukruak Entrance) is 10 times as wide: ~7.1 km. Another major inlet is at the eastern

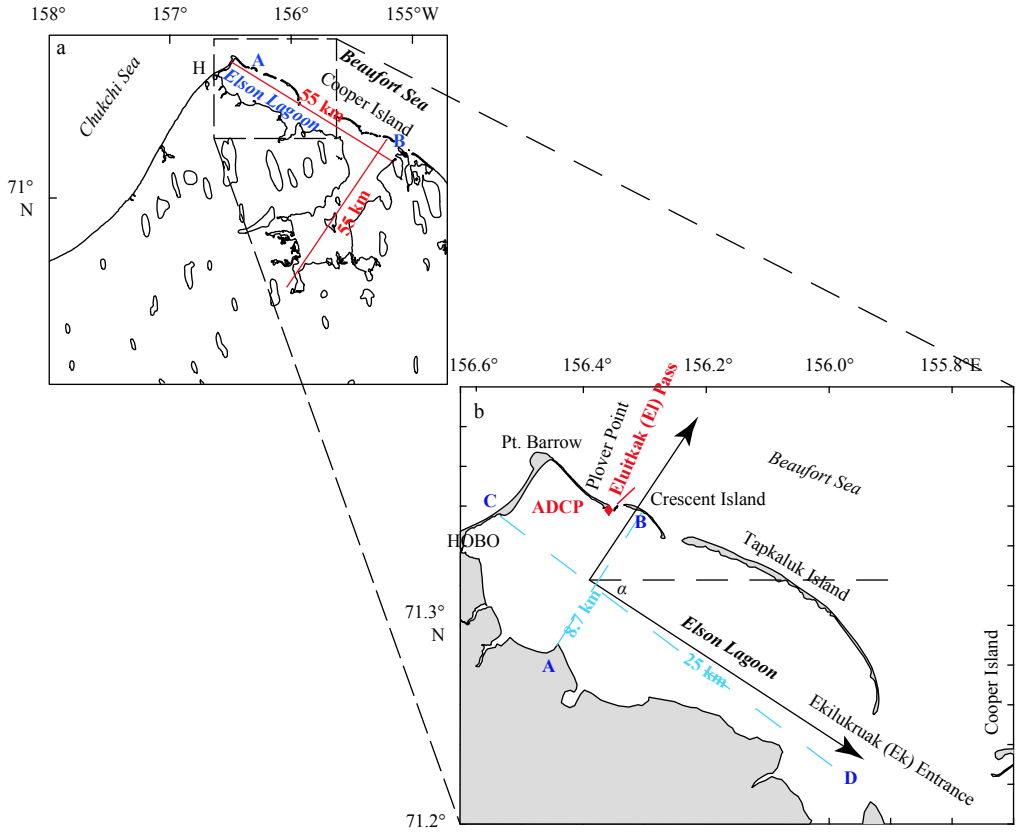

Fig. 1. Study area. The inset shows the position of the Elson Lagoon being at the corner of the Beaufort Sea and Chukchi Sea. The Elson Lagoon main axis is about –30° off the east-west direction. *H* on the inset marks the location of North Salt Lagoon. The North Salt Lagoon deployment site is also shown as HOBO in the zoomed-in map (without showing the lagoon because it is at the edge of the map).

end of the lagoon (marked as B in Fig. 1a).

In this area of the Alaska Arctic, the meso-scale atmospheric high- and low-pressure systems are frequent. Cyclones and anti-cyclones have a great impact on high-latitude communities and nearshore waters (Zhang et al., 2004). During summer time, the strong Beaufort Sea high usually centers over the Chukchi Sea and Beaufort Sea. They are mostly related to the Northern Annular Mode and the Pacific-North American teleconnection pattern (Wu et al., 2014). In between these high-pressure systems are low-pressure centers or cyclones (Serreze, 1997) or fronts separating different air masses, which can be associated with storms (Vavrus, 2013). The movement of these systems over the Arctic coastal areas causes the local wind to shift between northeasterly and westerly or northwesterly. The importance of wind to the ocean circulation, exchange between the lagoons and coastal ocean, and biological responses has long been recognized. The water exchange between the Elson Lagoon and the Beaufort Sea continental shelf was studied (Okkonen, 2008) with bottom mounted current meters measuring only the near bottom currents between August and September of 2006. The study found that the near bottom velocity was correlated with the east and west winds and some aggregations of zooplankton were found at the outflow fronts.

2.2 *Observations*

Aimed at determining the response of flow of water in and out of the Elson Lagoon with multiple inlets to winds of meso-scale cyclonic and anti-cyclonic weather systems, we deployed a RDI 1 200 kHz Broadband Workhorse acoustic Doppler current profiler (ADCP) at the Eluitkak Pass for approximately 4.9 days between 00:00 August 19 (Day 231 from January 1) and 20:48 UTC August 23 (Day 235), 2013 . The relatively short deployment is because of the frequent severe weather conditions, rough sea state, and potential damages of occasional floating ice. This instrument was deployed at 71°21.560′N, 156°21.152′W (Fig. 1), on a relatively flat bottom at 9.6 m depth, slightly east of the deepest water (~16 m) in the main channel. The ADCP was mounted on an aluminum cross comprised of four weighted legs. The ADCP was configured to record the three components of the velocity vector at 0.5 m vertical intervals every 60 seconds. Within each of the 60-second intervals, the ADCP sampled 50 times and provided an average for the ensemble.

In addition, a HOBO U20 Titanium Water Level Logger was deployed at about 0.5 m below the surface at the northern shore of the North Salt Lagoon at 71°20.459′N, 156°37.164′W. The North Salt Lagoon is an enclosed circular lake of ~1.3 km diameter connected to the Elson Lagoon at the south-western corner of the latter (Fig. 1). The U20 recorded data at 60 second intervals. This sensor was deployed in the North Salt Lagoon between 23:33 August 19 and 13:25 UTC August 23, 2013 . The U20 pressure sensor was used together with the pressure sensor on the ADCP to derive a pressure gradient, which is expected to vary with the wind direction and magnitude. The true water level variation was resolved with an atmospheric reference logger (Bosch BMP085) several km away at 71°16.522′N, 156°38.512′W, configured to sample at 0.5 Hz with an equivalent resolution of height change of 0.25 m in the air at an averaged sea level condition, or 0.306 mm of water level change at 4°C.

2.3 *Weather conditions*

Large-scale weather maps are obtained from NOAA (Fig. 2).

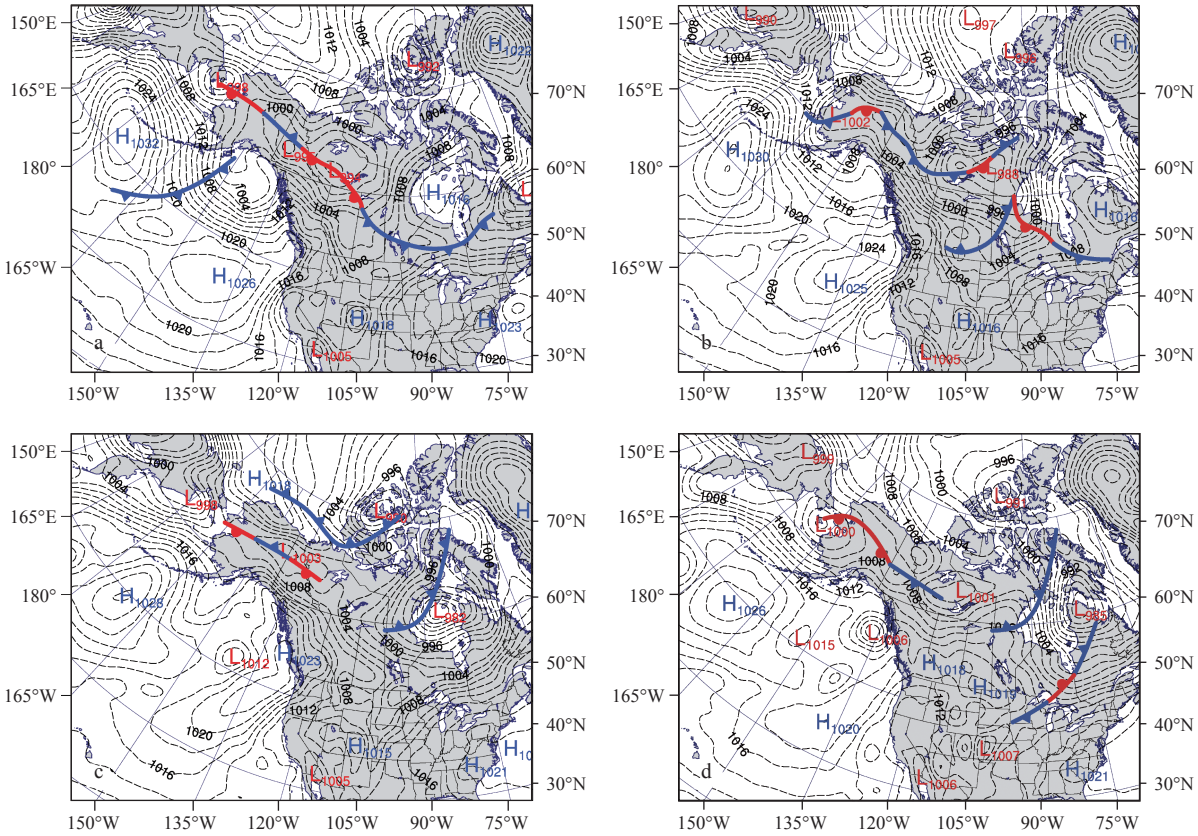

Fig. 2. Weather maps at (a) 00:00 UTC, August 19, 2013; (b) 00:00 UTC, August 20, 2013; (c) 03:00 UTC, August 21, 2013; (d) 00:00 UTC, August 22, 2013. Black dashed lines are isobars.

The meteorological conditions at the ADCP deployment (00:00 UTC August 19, 2013) were dominated by a low-pressure system (cyclone) located over the Bering Strait (sea-level air pressure ~999 hPa), with a linear stationary front connecting several low-pressure centers across Alaska into western Canada in a northwest-southeast orientation (Fig. 2a). Coincident with this was another low-pressure system located over Ellesmere Island in northern Canada (sea-level air pressure ~994 hPa). A high-pressure (anti-cyclone) system was juxtaposed to the north of the study area, in between these major low-pressure systems (a 1 018 hPa sea-level air pressure contour can be seen at top of Fig. 2a—note that the contour interval is 2 hPa), generating relatively strong northeasterly winds at the Elson Lagoon (Fig. 3). The northeasterly wind peaked before August 20 (Day 232, Fig. 3c). This condition (Fig. 2b) lasted for approximately a day as the systems gradually moved to the south (Fig. 2c). As a result, the high-pressure system moved over the study area (Fig. 2c). Concurrently, as the high-pressure system moved southeastward, the stationary atmospheric front developed into a couple of cold fronts occupying the Bering Strait and Western Alaska. At 03:00 UTC on August 21 (Day 233), the center of the high-pressure moved over the Barrow area and occupied there for less than 24 h (Fig. 2c). This is confirmed by the air pressure data recorded in Barrow (Fig. 3a). During this period, the measured wind intensity at the study area was weak (Fig. 3c, Day 233). As the low-pressure originally centered over the Ellesmere Island area moved to the south on August 22 (Day 234), pushing the high-pressure system away, the study area was under the influence of a persistent northwesterly wind (Fig. 2d). This variation in wind direction is typical for the area during the summer period with cyclones and anti-cyclones passing the region, resulting in variation in dominant wind directions (e.g., northeasterly to westerly or northwesterly). The change in wind direction can result in the presence or disappearance of floating ice in the area. The circulation with the presence of ice can be more complicated but is not discussed here.

3 Data processing and analysis

To examine the effect of wind velocity components in the along lagoon (northwest–southeast) and cross lagoon (northeast–southwest) directions, the wind vector is rotated 30° clockwise (Fig. 1b), so that a positive along lagoon wind is toward the southeast. The time series of rotated wind components during the study period are shown in Fig. 4a.

3.1 *Correction of water level for air pressure effect*

The air pressure data measured on land at intervals of 2 seconds are re-mapped to have the same time intervals of the HOBO U20 total pressure or water level data (i.e., 60 second intervals). For cross verification, we also use the air pressure data available from the nearby Barrow Airport (71.28°N, 156.79°W). The air pressure is subtracted from the total pressure measured by the HOBO sensor to calculate the water level (m), which is then de-meaned to obtain the water depth variation from the mean. The de-meaned time series is then low-pass filtered with a 30-hour sixth order Butterworth Infinite Impulse Response (IIR) filter (Emery and Thomson, 2004) which effectively removes the semi-diurnal tidal oscillations from the water level data. The 4.9 days of ADCP deployment encompassed about 9 semidiurnal tidal cycles. The averaged tidal range for that time period was about 0.2 m (Fig. 4), characteristic of a typical micro tidal system, and justifying the need to subtract the air pressure effect because of its relative significance due to the small variation of tides.

The ADCP also recorded water depth above the instrument. This water depth includes the effect of atmospheric pressure. A

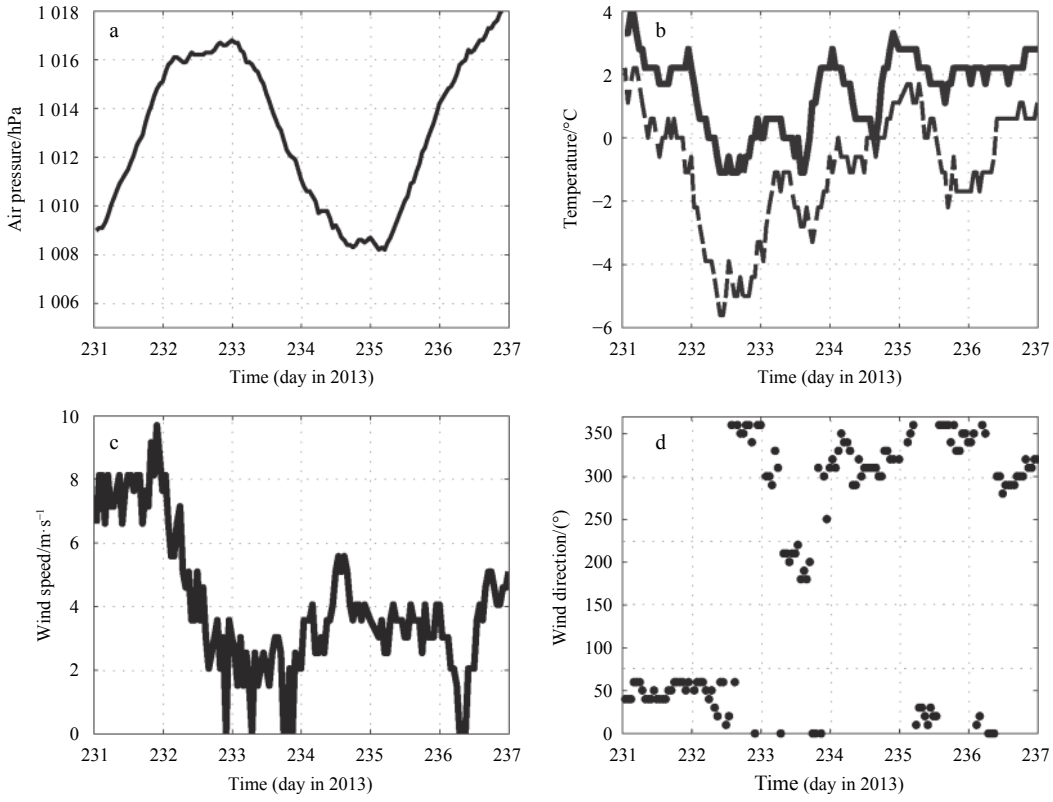

Fig. 3. Weather data. Air pressure (dashed line was from Barrow Airport) (a) air temperature (think line) and dew point temperature (dashed line) (b) wind speed (c) and wind direction (d).

similar procedure is applied to remove the air pressure effect on depth measured from the ADCP. The mean value of the water level over the entire study period of ~4.9 days is then subtracted. After this, the surface elevation measured by the ADCP (ζ_1) at Eluitkak Pass and that measured by the HOBO at the North Salt Lagoon (ζ_2) are used to calculate the difference of sea level anomaly:

$$\delta\zeta = \zeta_2 - \zeta_1. \tag{1}$$

Because these two stations are so close (~8 km), the mean sea level of the two are essentially the same, and the difference is caused by wind effect only.

3.2 *Low-pass filtering of the ADCP velocity data*

The water velocity data from the ADCP indicate a stronger along channel component than the cross-channel component, with the maximum cross channel velocity component being about 1/3 of that of the along channel component. Each component has detectable tidal signals. The velocity magnitude is generally larger near the water surface than that near the substrate, apparently because of bottom friction. The velocity at each level is also low-pass filtered by the 30-hour Butterworth filter. To avoid contaminated data near the surface due to the side-lobe effect of the transducers, the analysis of the velocity profile is restricted to below 9.36 mab (meters above bottom). The blue lines above the velocity contours in Figs 4c and d show the surface elevation measured by the ADCP's pressure sensor excluding the air pressure effect. The low-pass filtered along channel velocity component appears to have a variation very similar to that of the pressure difference ($\delta\zeta$) at all levels (Fig. 4b), indicating a strong linear correlation.

3.3 *Dynamic analysis of subtidal momentum equations*

To examine the statistical relationships between the wind and flow velocity, we now look at the two-dimensional momentum and continuity equations:

$$\frac{\partial u}{\partial t} + u\frac{\partial u}{\partial x} + v\frac{\partial u}{\partial y} - fv = -g\frac{\partial \zeta}{\partial x} + \frac{\tau_{ax}}{\rho(h+\zeta)} - \frac{\tau_{bx}}{\rho(h+\zeta)} - \frac{1}{\rho}\frac{\partial p_a}{\partial x}, \tag{2}$$

$$\frac{\partial v}{\partial t} + u\frac{\partial v}{\partial x} + v\frac{\partial v}{\partial y} + fu = -g\frac{\partial \zeta}{\partial y} + \frac{\tau_{ay}}{\rho(h+\zeta)} - \frac{\tau_{by}}{\rho(h+\zeta)} - \frac{1}{\rho}\frac{\partial p_a}{\partial y}, \tag{3}$$

$$\frac{\partial \zeta}{\partial t} + \frac{\partial (h+\zeta)u}{\partial x} + \frac{\partial (h+\zeta)v}{\partial y} = 0, \tag{4}$$

in which u, v, ζ, f, g, h, x, y, t, ρ, τ_{ax}, τ_{ay}, τ_{bx}, τ_{by} and p_a are the depth averaged east and north velocity, surface elevation, Coriolis parameter, gravitational acceleration, depth, east and north coordinates, time, water density, east and north wind stress components, east and north bottom stress components, and atmospheric pressure, respectively. In a rotated coordinate system, the new x-axis will be along the major axis of the lagoon (positive toward the southeast).

Each of the variables in the above equations should have a "high" frequency component (tidal or higher frequency oscillations) and the "low" frequency "subtidal" component. For ex-

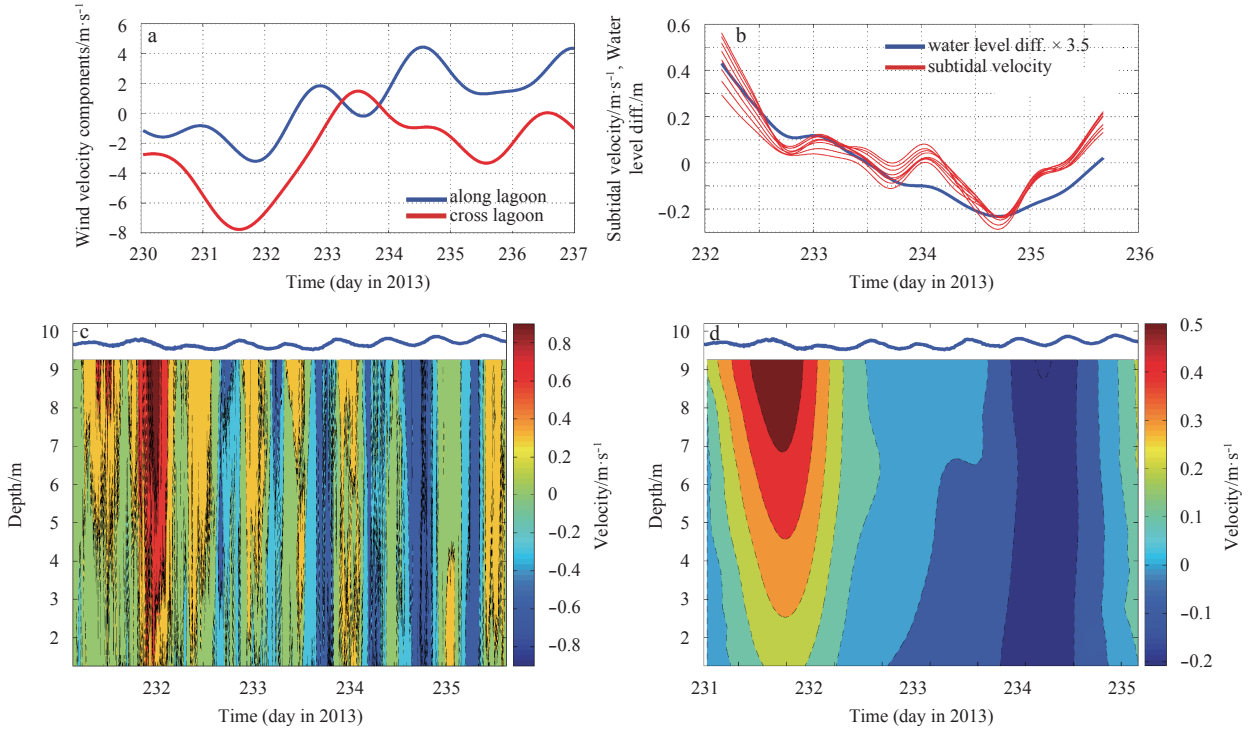

Fig. 4. Wind and flow. a. Wind velocity components along the lagoon (blue) and across (red); b. comparison of subtidal flow at various depths and the pressure difference (in meters, multiplied by 3.5 for visual comparison) between ADCP and HOBO sites; c. velocity profile time series: raw data and d.subtidal velocity profile time series.

ample, for velocity u and v, and water elevation ζ, they can be expressed as

$$u = u_H + u_L, v = v_H + v_L,\ \zeta = \zeta_H + \zeta_L. \tag{5}$$

The subscripts H and L denote the high frequency and low frequency, respectively.

If the two frequency regimes are "far apart" (with no overlaps), either of them can be effectively filtered out by a digital filter. Thus we can apply a low-pass filter to keep only the low-frequency or the so called subtidal component (e.g., u_L, v_L, ζ_L). It can be argued that for the first order approximation, the nonlinear advective terms can be neglected for convenience. We will however keep the nonlinear stress terms. The wind-driven subtidal motion can thus be expressed as:

$$\frac{\partial u_L}{\partial t} - f v_L = -g\frac{\partial \zeta_L}{\partial x} + \frac{\tau_{axL}}{\rho h} - \frac{\tau_{bxL}}{\rho h} - \frac{1}{\rho}\frac{\partial p_{aL}}{\partial x}, \tag{6}$$

$$\frac{\partial v_L}{\partial t} + f u_L = -g\frac{\partial \zeta}{\partial y} + \frac{\tau_{ayL}}{\rho h} - \frac{\tau_{byL}}{\rho \mathrm{h}} - \frac{1}{\rho}\frac{\partial p_{aL}}{\partial y}, \tag{7}$$

$$\frac{\partial \zeta_L}{\partial t} + \frac{\partial h u_L}{\partial x} + \frac{\partial h v_L}{\partial y} = 0. \tag{8}$$

We can now do a quick order-of-magnitude estimate based on our data (Fig. 4). The variation in u_L, v_L is ~0.6 m/s over 3 days, while the change in ζ_L is ~0.17 m over 3 days. Consider that the lagoon has a width of ~8 km, we can estimate that $\frac{\partial u_L}{\partial t}$ and $\frac{\partial v_L}{\partial t}$ are ~2.3×10^{-6} m/s^2, and $g\frac{\partial \zeta_L}{\partial x}$ is ~2.1×10^{-4} m/s^2. This tells us that the local rate of change of the subtidal flow components are two orders of magnitude smaller than the subtidal pressure gradient force terms. Therefore, we can use the following approximate momentum equations:

$$-f v_L = -g\frac{\partial \zeta_L}{\partial x} + \frac{\tau_{axL}}{\rho h} - \frac{\tau_{bxL}}{\rho h} - \frac{1}{\rho}\frac{\partial p_{aL}}{\partial x}, \tag{9}$$

$$f u_L = -g\frac{\partial \zeta}{\partial y} + \frac{\tau_{ayL}}{\rho h} - \frac{\tau_{byL}}{\rho \mathrm{h}} - \frac{1}{\rho}\frac{\partial p_{aL}}{\partial y}. \tag{10}$$

The wind stress is

$$\boldsymbol{\tau}_a = \rho_a C_{Da} \boldsymbol{w} |\boldsymbol{w}|, \tag{11}$$

in which $\boldsymbol{\tau}_a = (\tau_{ax}, \tau_{ay})$ is the wind stress vector, C_{Da} is the wind drag coefficient on the ocean surface, $\mathbf{w}$=(w_x, w_y) is wind velocity vector, and ρ_a is the air density.

Equations (6), (7), and (8) have three unknowns (u_L, v_L, ζ_L). With proper boundary and initial conditions, a solution can be obtained for the unknowns. However, with the complicated bathymetry, coastlines, and temporally and spatially varying forcing factors, it is almost impossible to obtain an exact and general (or even a special) solution. We now seek to derive a possible relationship between the forcing (wind) and response (velocity), which can be used for a statistical regression.

Any solution for (u_L, v_L, ζ_L) can be expressed in theory by the general format:

$$u_L = u_L\left(\Delta p_{aL}, \tau_{axL}, \tau_{ayL}\right), \tag{12}$$

$$v_L = v_L\left(\Delta p_{aL}, \tau_{axL}, \tau_{ayL}\right), \tag{13}$$

$$\zeta_L = \zeta_L\left(\Delta p_{aL}, \tau_{axL}, \tau_{ayL}\right), \tag{14}$$

in which the air pressure anomaly $\Delta p_{aL} = p_{aL} - p_{aL0}$, where p_{aL0} is the background or environmental air pressure or the average air pressure at sea level. Again, the subscript L indicates a low-pass filtered quantity. Note that the Coriolis force is included for completeness. If the Coriolis effect is negligible, the format of the above solution and Eqs (12)–(14) still remain the same. Now we do a Taylor series expansion for the above equations in terms of the variables Δp_a, τ_{ax} and τ_{ay} to the first order:

$$u_L = u_L(0,0,0) + \frac{\partial u_L}{\partial p_{aL}}\Delta p_{aL} + \frac{\partial u_L}{\partial \tau_{axL}}\tau_{axL} + \frac{\partial u_L}{\partial \tau_{ayL}}\tau_{ayL}, \tag{15}$$

$$v_L = v_L(0,0,0) + \frac{\partial v_L}{\partial p_{aL}}\Delta p_{aL} + \frac{\partial v_L}{\partial \tau_{axL}}\tau_{axL} + \frac{\partial v_L}{\partial \tau_{ayL}}\tau_{ayL}, \tag{16}$$

$$\zeta_L = \zeta_L(0,0,0) + \frac{\partial \zeta_L}{\partial p_{aL}}\Delta p_{aL} + \frac{\partial \zeta_L}{\partial \tau_{axL}}\tau_{axL} + \frac{\partial \zeta_L}{\partial \tau_{ayL}}\tau_{ayL}. \tag{17}$$

All the derivatives in Eq (15), (16) and (17) are evaluated at (0, 0, 0) for $(\Delta p_{aL}, \tau_{axL}, \tau_{ayL})$. In the above equations, the wind stress terms can be further expressed by wind velocity components, i.e., for the wind stress itself, similar to the quadratic bottom friction, a Taylor series expansion (e.g., Proudman, 1953; Parker, 1984) can be used to express the stress in terms of a linear term and a higher order nonlinear term, i.e.,

$$\tau_{axL} = \alpha w_x + \beta w_x^2 + \text{higher order terms}, \tag{18}$$

$$\tau_{ayL} = \gamma w_y + \delta w_y^2 + \text{higher order terms}, \tag{19}$$

where α, β, γ, δ are all constants of the Taylor series expansions. Substitute Eqs (18) and (19) into Eqs (15)–(17) and neglect the higher order terms we obtain:

$$u_L = u_L(0,0,0) + \frac{\partial u_L}{\partial p_{aL}}\Delta p_{aL} + \frac{\partial u_L}{\partial \tau_{axL}}\left(\alpha w_x + \beta w_x^2\right) + \frac{\partial u_L}{\partial \tau_{ayL}}\left(\gamma w_y + \delta w_y^2\right), \tag{20}$$

$$v_L = v_L(0,0,0) + \frac{\partial v_L}{\partial p_{aL}}\Delta p_{aL} + \frac{\partial v_L}{\partial \tau_{axL}}\left(\alpha w_x + \beta w_x^2\right) + \frac{\partial v_L}{\partial \tau_{ayL}}\left(\gamma w_y + \delta w_y^2\right), \tag{21}$$

$$\zeta_L = \zeta_L(0,0,0) + \frac{\partial \zeta_L}{\partial p_{aL}}\Delta p_{aL} + \frac{\partial \zeta_L}{\partial \tau_{axL}}\left(\alpha w_x + \beta w_x^2\right) + \frac{\partial \zeta_L}{\partial \tau_{ayL}}\left(\gamma w_y + \delta w_y^2\right). \tag{22}$$

These can be rewritten as:

$$u_L = Aw_x + Bw_x^2 + Cw_y + Dw_y^2 + E\Delta p_a + F, \quad (23)$$

$$v_L = Gw_x + Hw_x^2 + Iw_y + Jw_y^2 + K\Delta p_a + L, \quad (24)$$

$$\zeta_L = Mw_x + Nw_x^2 + Ow_y + Pw_y^2 + Q\Delta p_a + R, \quad (25)$$

in which, $A = \alpha \frac{\partial u_L}{\partial \tau_{axL}}$, $B = \beta \frac{\partial u_L}{\partial \tau_{axL}}$, $C = \gamma \frac{\partial u_L}{\partial \tau_{avL}}$, $D = \delta \frac{\partial u_L}{\partial \tau_{avL}}$, $E = \frac{\partial u_L}{\partial p_{aL}}$, $F{=}u_L(0, 0, 0)$, $G = \alpha \frac{\partial v_L}{\partial \tau_{axL}}$, $H = \beta \frac{\partial v_L}{\partial \tau_{axL}}$, $I = \gamma \frac{\partial v_L}{\partial \tau_{avL}}$, $J = \delta \frac{\partial v_L}{\partial \tau_{ayL}}$, $K = \frac{\partial v_L}{\partial p_{aL}}$, $L{=}v_L(0, 0, 0)$, $M = \alpha \frac{\partial \zeta_L}{\partial \tau_{axL}}$, $N = \beta \frac{\partial \zeta_L}{\partial \tau_{axL}}$, $O = \gamma \frac{\partial \zeta_L}{\partial \tau_{ayL}}$, $P = \delta \frac{\partial \zeta_L}{\partial \tau_{ayL}}$, $Q = \frac{\partial \zeta_L}{\partial p_{aL}}$, $R{=}\zeta_L(0, 0, 0)$. It should be noted that this is not an explicit solution as the coefficients are all unknowns. However, Eqs (23), (24), and (25) suggest that the low-pass filtered velocity and elevation are linearly related to air pressure anomaly, the wind speed components, and their squares, which we will utilize in the next section for a regression analysis.

3.4 *Regression analysis*

From the above discussion and derivation, the following regression equation is used:

$$u(t) = AW_a(t) + BW_a^2(t) + CW_c(t) + DW_c^2(t) + E, \quad (26)$$

in which $u(t)$, $W_a(t)$, $W_c(t)$ are, respectively, the time series of the low-pass filtered outward component of the velocity (positive outward) at Eluitkak Pass, the along-lagoon wind velocity component (positive toward the southeast), and the cross-lagoon wind velocity component (positive toward the northeast). *A, B, C, D*, and *E* are the regression coefficients. Note that in Eq (26), we ignored the air pressure terms, which are found to be negligible compared to the wind velocity component terms. We nevertheless keep these terms in Eqs (23)–(25) in case for different applications they might be more important. The discussion can be extended to 3-D problems and Eq (26) can be applied to data at different depths.

The results indicate that the subtidal velocity is correlated to and apparently largely determined by wind velocity. When the north-northeasterly wind reaches its maximum, just prior to day 232 (August 20) (Fig. 5), the water velocity is also at a maximum, indicating a current going out of the lagoon against the wind. When the wind switches to westerly and northwesterly on Day 235 (August 23), the velocity reverses its direction. The R^2 values at all depths are high (all above 0.9, Table 1). The signs of the regression coefficients (*A, B, C, D*, and *E*) are all consistent at different depths. For example, *A* is always negative, meaning that a negative along-lagoon wind will contribute a positive outward flow at the Eluitkak pass. Likewise, *C* is negative, meaning a northeasterly wind will contribute a counter-wind flow (outward flow) at the pass and vice versa.

The fact that a northeasterly wind causes a northeasterly flow (out of the lagoon) through the narrower inlet verifies this idea: water in the wider openings at the eastern Elson Lagoon receive more acceleration under roughly the same wind stress due to its shallow water and broad opening; while the much narrower opening at the northwestern end receives much less forcing from the wind stress and less easier to accelerate by wind due to its much deeper water and much narrower width for the integrated wind forcing across the inlet. The barrier islands can effectively block the flow and therefore wind stress need not to be considered there for the purpose of water transport through the inlets. The larger wind forcing at the larger openings, especially the major eastern inlet (B on Fig. 1a), will tend to produce a flow in the direction of wind; only to be balanced by a return flow through the Eluitkak Pass. This can also be explained from a vorticity or torque point of view: the large wind forcing for transport in the eastern inlets than the northwestern inlet causes a "torque" similar to that discussed by Engelund (1986), Fischer (1976), and Li (2013). In other words, the wind pushes water into the lagoon from the wider openings on the eastern end, generating a higher water level on the eastern side, causing a pressure gradient induced flow to exit the lagoon through the northwestern narrow inlet, the Eluitkak Pass.

Other factors that can affect the exchange flow such as coastal current and river discharge apparently have less importance than wind in this case. This is most likely because the system is semi-enclosed by a series of barrier islands, making the integrated wind effect at the narrow tidal pass amplified. The method presented here is for ice-free conditions in the summer. With a significant presence of floating ice, the exchange flows may be affected.

4 Numerical experiments of wind driven flow

The above analysis suggests the existence of counter-wind

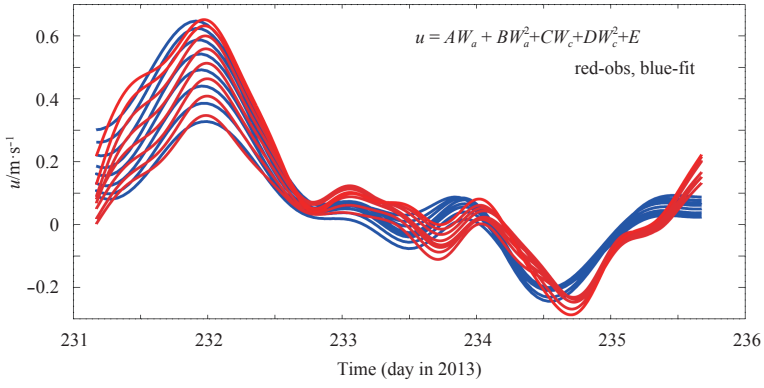

Fig. 5. Comparison of observed and regression model produced subtidal flows in and out of the lagoon (positive out of the lagoon onto the shelf). Red lines are from observations and blue lines are from the regression.

Table 1. Regression of subtidal velocity with wind velocity components and their squares for the entire time period when the ADCP was measuring velocity

H/mab	Regression coefficient *A, B, C, D, E*	95% confidence interval C		R^2
9.36	−0.045 8	−0.046 2	−0.045 4	0.962 8
	0.000 4	0.000 4	0.000 4	
	−0.012 5	−0.013 2	−0.011 8	
	−0.003 8	−0.003 9	−0.003 7	
	0.170 2	0.167 7	0.172 6	
8.36	−0.044 3	−0.044 6	−0.043 9	0.959 1
	0.000 5	0.000 5	0.000 5	
	−0.016 9	−0.017 6	−0.016 2	
	−0.004 5	−0.004 6	−0.004 4	
	0.165 2	0.162 8	0.167 7	
7.36	−0.041 6	−0.042 0	−0.041 2	0.947 0
	0.000 6	0.000 5	0.000 6	
	−0.020 4	−0.021 1	−0.019 7	
	−0.004 9	−0.005 0	−0.004 8	
	0.159 5	0.157 0	0.162 1	
6.36	−0.039 5	−0.039 9	−0.039 1	0.932 4
	0.000 5	0.000 5	0.000 6	
	−0.023 3	−0.024 1	−0.022 6	
	−0.005 2	−0.005 3	−0.005 1	
	0.147 6	0.144 8	0.150 3	
5.36	−0.037 6	−0.038 0	−0.037 3	0.928 2
	0.000 4	0.000 4	0.000 5	
	−0.022 0	−0.022 7	−0.021 3	
	−0.004 9	−0.005 0	−0.004 8	
	0.132 5	0.129 9	0.135 1	
4.36	−0.036 0	−0.036 3	−0.035 6	0.931 3
	0.000 3	0.000 3	0.000 3	
	−0.021 4	−0.022 0	−0.020 8	
	−0.004 8	−0.004 9	−0.004 7	
	0.119 6	0.117 2	0.121 9	
3.36	−0.033 9	−0.034 2	−0.033 6	0.934 9
	0.000 2	0.000 1	0.000 2	
	−0.021 9	−0.022 4	−0.021 3	
	−0.004 6	−0.004 7	−0.004 5	
	0.099 5	0.097 5	0.101 6	
2.36	−0.031 3	−0.031 6	−0.031 1	0.937 6
	−0.000 0	−0.000 0	0.000 0	
	−0.021 5	−0.022 1	−0.021 0	
	−0.004 1	−0.004 2	−0.004 1	
	0.071 0	0.069 2	0.072 9	

flows in the narrow Eluitkak Pass. In addition, the prismatic lake model of Engelund (1986) of wind-driven flows is applicable here and the scenarios of wind-driven flows through multiple inlets (Li, 2013) appear to be relevant. However, the observations are limited to 4.9 days. Because of the logistic challenges, longer observations, albeit desired, are difficult to accomplish. It is therefore necessary to use a numerical model to corroborate the findings, to provide a better picture of the circulation in the system, and to aid the examination of the dynamic process.

4.1 *Delft3D-FLOW setup*

The Delft3d-FLOW model is used to simulate wind-driven circulation in Elson Lagoon and Eluitkak Pass. The model domain for the Delft3D contains a 555×279 curvilinear orthogonal grid in the horizontal which extends from 154.56°W to 156.48°W and 71.25°N to 71.53°N (Fig. 6). Grid resolution varies between roughly 20 m and 2.5 km. The bathymetry data are obtained from the National Geophysical Data Center (NGDC) with the approximate spatial resolution of 90 meters (www.ngdc.noaa.gov/mgg/coastal/crm.html) and our own measurements in the Eluitkak Pass in August 2013. The time step Δt is set to 0.1 minute. The vertical discretization is based on sigma coordinate with 5 layers.

Tidal constituents at the open boundary are extracted from the US Army Corps of Engineers regional ADCIRC model (Westerink et al., 1993). The model is forced by spatially uniform and temporally variable winds obtained from the Barrow Airport station (71.28°N, 156.79°W) managed by the National Climatic Data Center (NCDC).

4.2 *Model validation*

The numerical model reproduces tides and tidal currents consistent with the observations, especially considering the small magnitude of tides in this micro-tidal region (Fig. 7). The com-

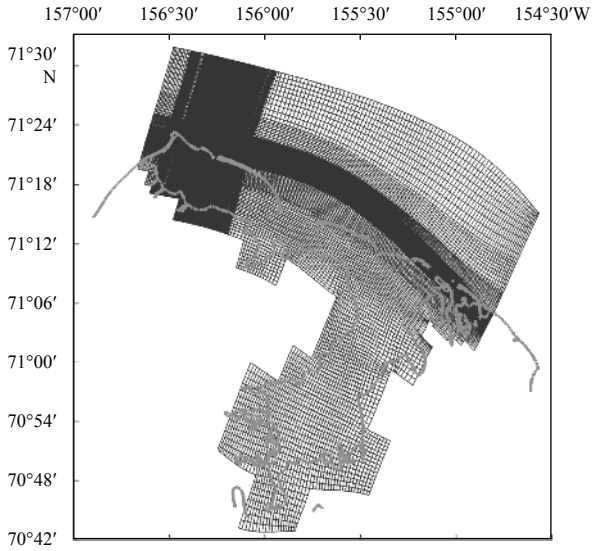

Fig. 6. The 555×279 curvilinear orthogonal model grid, the mesh resolution varies from 2.5 km and 45 m.

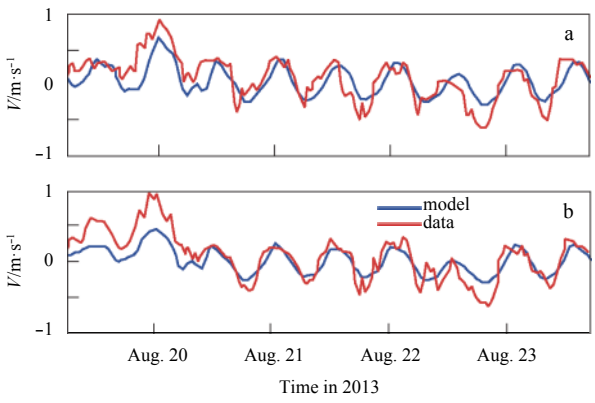

Fig. 7. Model-data comparison of along channel velocity component. Black line is from model and red line is from data. *V*-velocity component near-surface velocity (a), near-bottom velocity (b) at ADCP location between August 19 and August 24, 2013.

parison between model results and measured current velocity time series is made at the ADCP site at 71.35°N, 156.35°W. The model captures tidal currents in and out of the inlet as well as the effect of wind. There is however some discrepancies, most likely caused by possible errors in bathymetry. This study site is remote and has no supporting facility for extensive survey operations and thus bathymetry data are very limited, both inside and outside of the lagoon. Our measurements of water depth mainly covered the channel at the Eluitkak Pass and inside the lagoon where water depth has been measured by acoustic sensors on a boat mounted ADCP or an unmanned vehicle.

4.3 *Numerical experiments*

To quantify the effect of various wind directions on the exchange flows through Eluitkak Pass and Elson Lagoon, we have designed and conducted a series of numerical experiments (Table 2) with this model. Considering the predominant wind conditions of the area, the experiments included easterly, northeasterly, and northwesterly winds. The wind speed is assumed in the model linearly increasing from 2 m/s to 15 m/s within 15 days for each of the three wind directions (Table 2).

Under easterly wind, the northwestern inlet (the narrow Eluitkak Pass) shows outward flows while the eastern inlets (including the wider Ekilukruak Entrance) show inward flows (near

Table 2. Numerical model experiments

Wind direction	Wind speed	Exchange flows
Easterly	Linearly increasing from 2 to 15 m/s in 15 d	Outward flow through Eluitkak Pass, inward flows through the southeastern inlets
Northeasterly	(same as above)	Outward flow through Eluitkak Pass, inward flows through the southeastern inlets
Northwesterly	(same as above)	inward flow through Eluitkak Pass, outward flows through the southeastern inlets

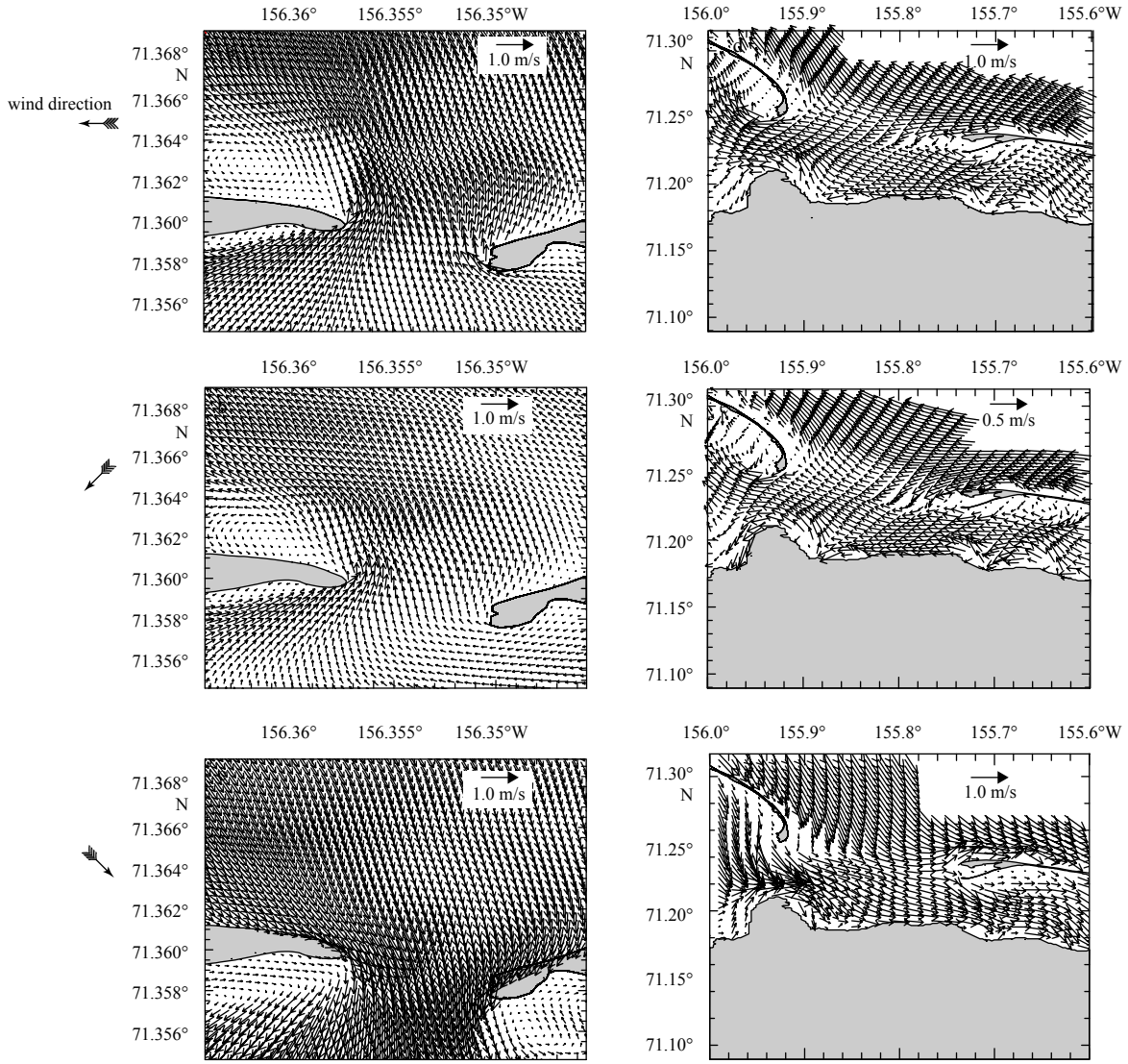

Fig. 8. Numerical model output for the flows at the Eluitkak Pass under east (a), northeast (b) and northwest winds (c), respectively; and those at the Ekilukruak Entrance under east (d), northeast (e) and northwest (f) winds, respectively.

surface flows in Figs 8a and d). Under northeasterly wind, the Eluitkak Pass also has outward flows and the eastern inlets inward flows (Figs 8b and e). The outward flow through the northwestern inlet is smaller in magnitude, but still against the wind. Under northwesterly wind, the Eluitkak Pass has inward flows while the eastern inlets have outward flows (Figs 8c and f).

When the wind speed varies from 2 to 15 m/s linearly over 15 days, the water level difference between the HOBO site (Fig. 1b) and ADCP site varies. Under east wind, this water level difference (m) is positive (water level at HOBO site is higher than that at the ADCP site), consistent with an outward flow (Fig. 9a). This is confirmed by Fig. 4b of the observed water level difference. The actual magnitude from measurement is about 0.17 m between the HOBO site and ADCP site. This value is comparable to the maximum magnitude of ~0.16 from the model (Fig. 9a). The water level difference between Point A (Fig. 1b) and ADCP site is smaller for the east wind condition. For the northeast (Fig. 9b) and north winds (Fig. 9c), the water level differences are similar which are all consistent with outward flows at the Eluitkak Pass. For the northwest wind case (Fig. 9d), the water level difference between the HOBO and ADCP sites changes sign, indicating a tendency of inward flows. The water level at Point A is slightly higher than that at the ADCP site. These results from the numerical experiment are all consistent with the regression analysis using the *in situ* data.

4.4 *Adjustment and quasi-steady state balance*

In a one-dimensional channel with a closed end in the downwind direction, and under a constant wind forcing towards the closed end, the steady-state force balance would be

$$0 = -g\frac{\partial \zeta}{\partial x} + \frac{\tau_{ax}}{\rho h}. \tag{27}$$

If the wind varies in magnitude and direction, or if the water cannot be viewed as "one-dimensional", or if the end is not fully closed (e.g., with a narrow inlet allowing water flowing in or out), the above force balance would not hold and a local acceleration would have to be included. A two-dimensionality of motion would also invalidate the above equation. In Huang and Li (2017) however, it is shown that the above balance for subtidal variation is quite accurate even when wind is changing.

Li et al. (2018a) further investigated the adjustment of wind-driven flows and demonstrated that a change in wind will produce damped oscillations similar to the solution of:

$$m\frac{\mathrm{d}^2 y}{\mathrm{d}t^2} + 2mr\frac{\mathrm{d}y}{\mathrm{d}t} + m\omega_0 y = f(t), \tag{28}$$

where m, r, ω_0 are all constants, t is time, y is the dependent variable (here the water slope), and $f(t)$ is the forcing function. The solution is a forced damped oscillation in a form like

$$y = ce^{-rt}\sin\left(\sqrt{\omega_0^2 - r^2}\,t + \delta\right) + G(t), \tag{29}$$

where the first term on the right-hand side is a free damped function and the second term G a convolution between the wind stress and surface slope. The G function contains various frequencies but only the one that matches the natural oscillation frequency of the system will be significant. The fundamental seiche period of the system is defined by

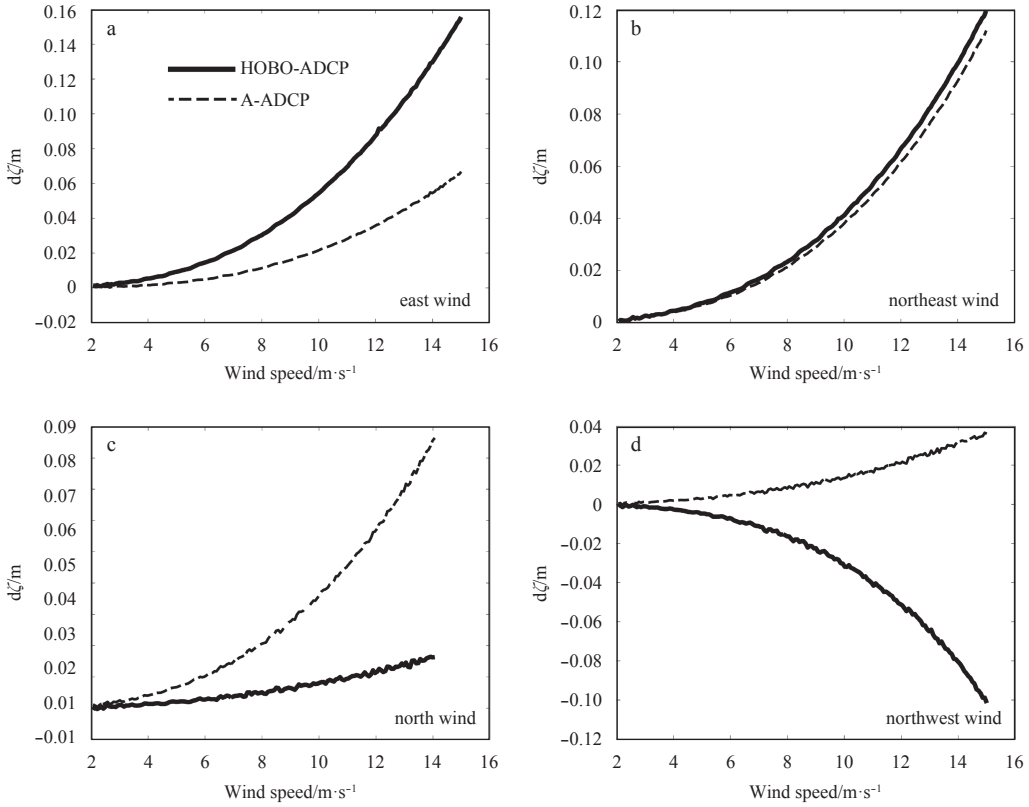

Fig. 9. Water level difference (m) between the HOBO pressure site and the ADCP deployment site (solid lines); and that between Point A and ADCP site (dashed lines) for the idealized numerical experiment in which wind is varied from 2 m/s to 15 m/s linearly over 15 days: east wind (a); northeast wind (b); north wind (c); northwest wind (d).

$$T = \frac{2L}{\sqrt{gh}}, \tag{30}$$

where T, L, g and h are the period of seiche oscillation, the distance between two reflection points on opposite coasts, gravitational acceleration, and mean water depth, respectively. The damped seiche oscillation only lasts for 2–3 cycles, each for ~3 hours, adjusting the system to a new balance, leading to a quasi-steady state (Li et al., 2018a). Because of this quasi-steady state balance, the wind and the subtidal flow at the narrow pass are highly correlated. In comparison, Eqs (9) and (10) neglect the local accelerations because they are small in the subtidal regime. These two viewpoints give consistent conclusion that wind-driven flows in such multiple inlet lagoon system is under quasi-steady state balance even if the wind varies with time.

Using the numerical model results for the calculation between August 15 and 26, 2013, we compare the results between the numerical model and that from the quasi-steady state Eq. (27). The quantity for comparison is the water level difference, between Points A and B (Fig. 1b), and that between Points C and D—one represents the cross-lagoon water level difference (between A and B), the other represents the along-lagoon difference (between C and D). The numerical model produces cross-lagoon water level difference and that calculated from Eq. (27) are again quite consistent. The two follow each other in both magnitude and phase (Fig. 10a). The correlation coefficient of the two is 0.62. Because the wind data are noisy, there are some small magnitude random variations. After a 30-hour low-pass filtering, the correlation coefficient increases to 0.82 (Fig. 10b). The along-lagoon water level difference from the model and that calculated from Eq. (27) are also consistent. The two follow each other (Fig. 10c). The correlation coefficient of the two is about 0.55, slightly smaller than that for the cross-lagoon water level difference. After a 30-hour low-pass filtering, the two again have better correlation with a coefficient of 0.71 (Fig. 10d).

It is clear that the water level variations within the Elson Lagoon are largely wind-driven. It is quite remarkable to have such a good agreement between the modeled water level difference and that from the quasi-steady state balance. This is consistent with the recent studies in similar semi-enclosed shallow water systems with micro-tides (Huang and Li, 2017; Li et al., 2018b).

4.5 *Wind-driven flows in a multiple inlet lagoon*

The subject of study here involves a multiple inlet lagoon system. This kind of system is different from a conventional estuary with a single opening. Wind-driven flows through a multiple inlet system has been found to be characterized by inward flows from some inlets, balanced by outward flows from other inlets, depending on the wind condition, bathymetry, depth ratios, and width ratios. It is found (Li, 2013) that when wind is perpendicular to the coast, the shallower inlet tends to have downwind flow while the deeper inlet might have an upwind flow, or at least a weaker downwind flow. In contrast, the middle inlet tends to be weakest in flow magnitude and less defined in direction. When the wind is not perpendicular to the coast with an onshore component, the outward flow usually occurs at the inlet that is farther away in the downwind direction, compensated by an inward flow in an inlet at an upwind location. These are confirmed in the present numerical model results. The counter-wind flows in the deep inlet is one example. Another example is that the middle inlet tends to have minimum flow and less defined in flow directions (Fig. 11). Under easterly wind, which is quite common in the arctic region because of the high-pressure systems in the

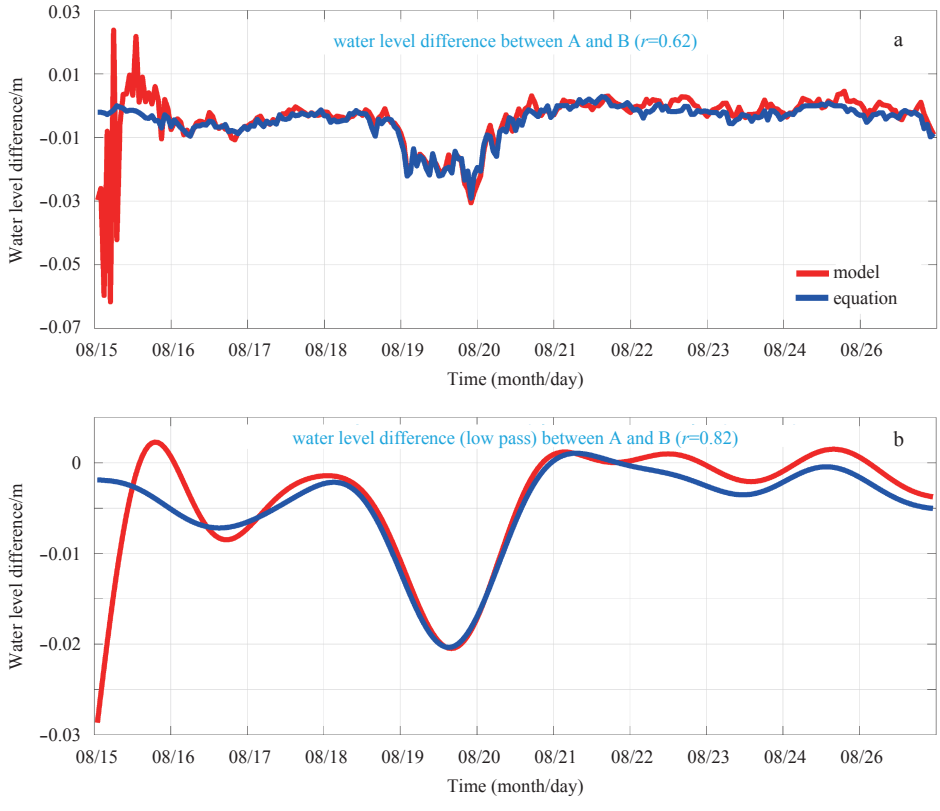

Fig. 10.

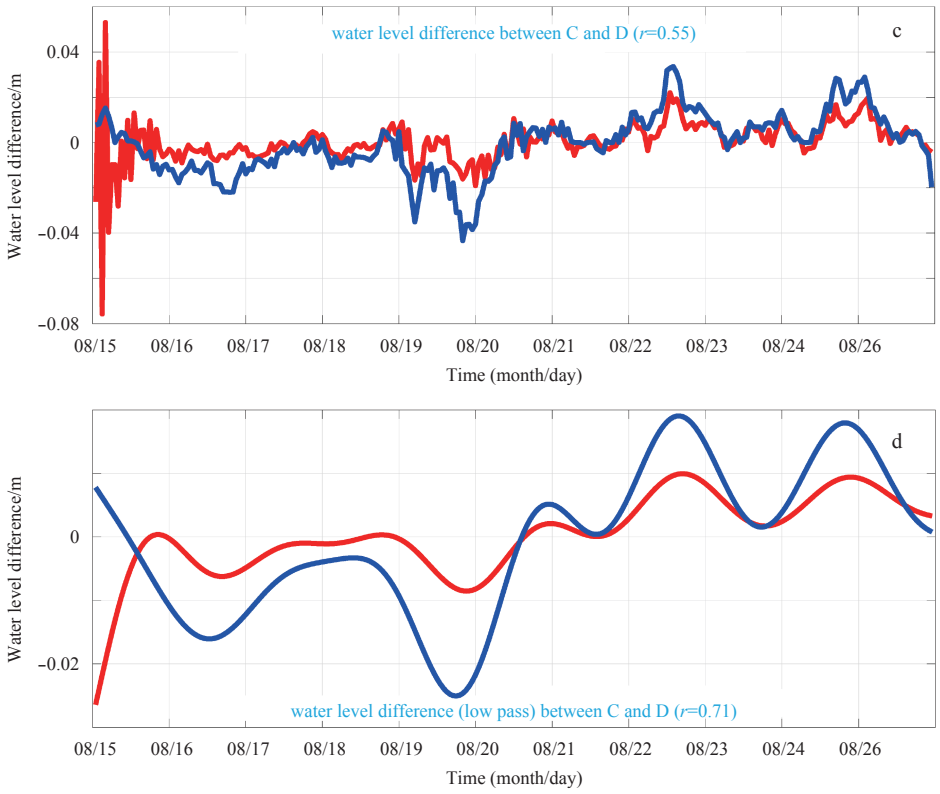

Fig. 10. Comparison between the numerical model results and the quasi-steady state force balance. Water level difference between A and B (Fig. 1b) from the model (red line) and that from the quasi-steady state balance, i.e, Eq. (27) (blue line) (a). Same as (a) except for low-pass filtered version (b). Water level difference between C and D (Fig. 1b) from the model (red line) and that from Eq. (27) (blue line) (c). Same as (c) except for low-pass filtered version (d).

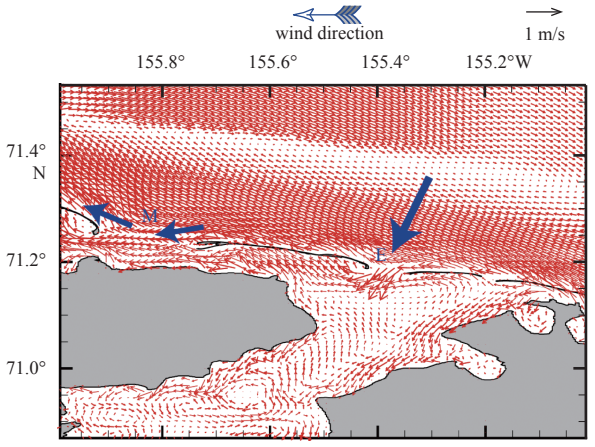

Fig. 11. Wind-driven flows through the easternmost inlet, compared with that through the wider middle inlet, under the commonly occurring easterly winds. M is the widest middle inlet and E the major eastern inlet. The red arrows are the surface velocity vectors, while the thick blue arrows indicate the general directions and magnitude at the M and E inlets.

higher latitude, strong inward flows are shown to occur at the major eastern inlet (marked with E in Fig. 11), while the flows through the middle inlet (marked with M in Fig. 11) appear to be just skimming along the coastline with a limited inward flow. We do not have data at the eastern inlets. However, the validated model provides results consistent with characteristic flow patterns in a multiple inlet lagoon.

5 Discussion and summary

5.1 *Landsat-8 OLI images*

To further examine our findings, satellite images are sought for signatures of water plumes that may indicate the exchange flows in and out of the Elson Lagoon. We have particularly searched for high-resolution images from Landsat data. We could only find two images after our 2013 field campaign. They are two orthorectified and terrain corrected Landsat-8 OLI Level 1T images in GeoTIFF format obtained from the U.S. Geological Survey (USGS) Earth Explorer portal (https://earthexplorer.usgs.gov/) for the study area on July 7, 2015 (Figs 12a–c) and July 12, 2017 (Figs 12d–f) at 22:18:29 UTC. Landsat-8 was launched on February 11, 2013 and became operational on May 30, 2013. The 30-m high spatial resolution images help to identify the patterns of inflow and outflow through the Elson Lagoon inlets. The ACOLITE (version 20170718.0) software package (https://odnature.naturalsciences.be/remsem/software-and-data/acolite) is used to make corrections for the Rayleigh scattering. On July 7, 2015, there was a high-pressure atmospheric system north of the study area over the Beaufort Sea region. The system brought a northeasterly wind over Elson Lagoon (Fig. 13a). The Landsat-8 OLI image shows that the coastal water appears to be coming into the Elson Lagoon through the wider southeastern inlets (Figs 12a and c); while a plume of turbid water can be seen going out of the Elson Lagoon from the Eluitkak Pass (Figs 12a and b). On July 12, 2017, the atmospheric system did not change much and the predominant wind over the Elson Lagoon area was easterly (Fig. 13b).

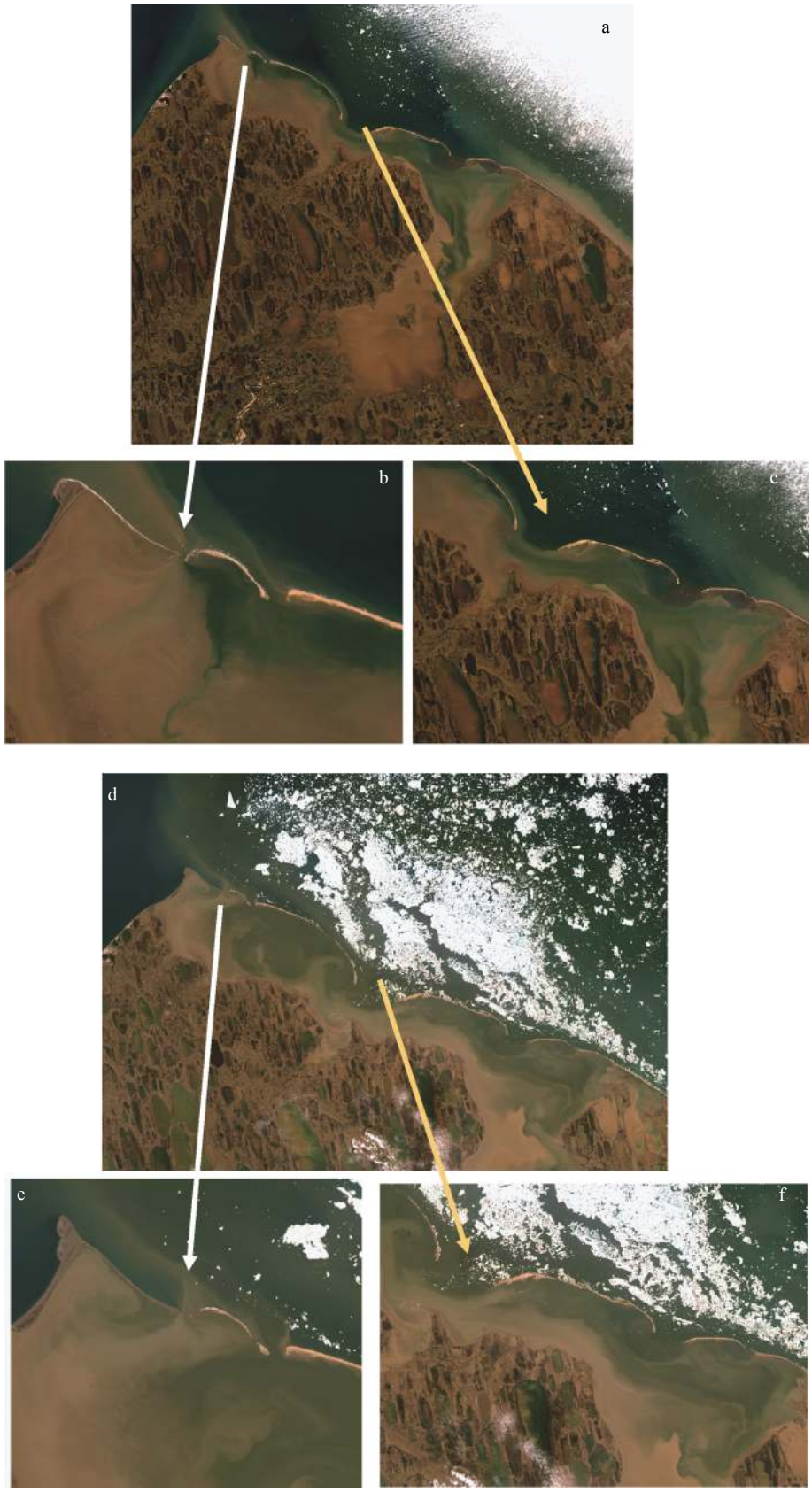

Fig. 12. A Rayleigh corrected true Landsat-8 OLI image obtained on 7 July 2015 at 22:18:29 UTC (a–c). A Rayleigh corrected true Landsat-8 OLI image obtained on July 12, 2017 at 22:18:29 UTC (d–f).

The Landsat image shows again some coastal water coming into Elson Lagoon through the wider inlets (clear water on Figs 12d and f); while a plume of turbid water is seen going out of the Elson Lagoon through the Eluitkak Pass (Figs 12d and e). It can be

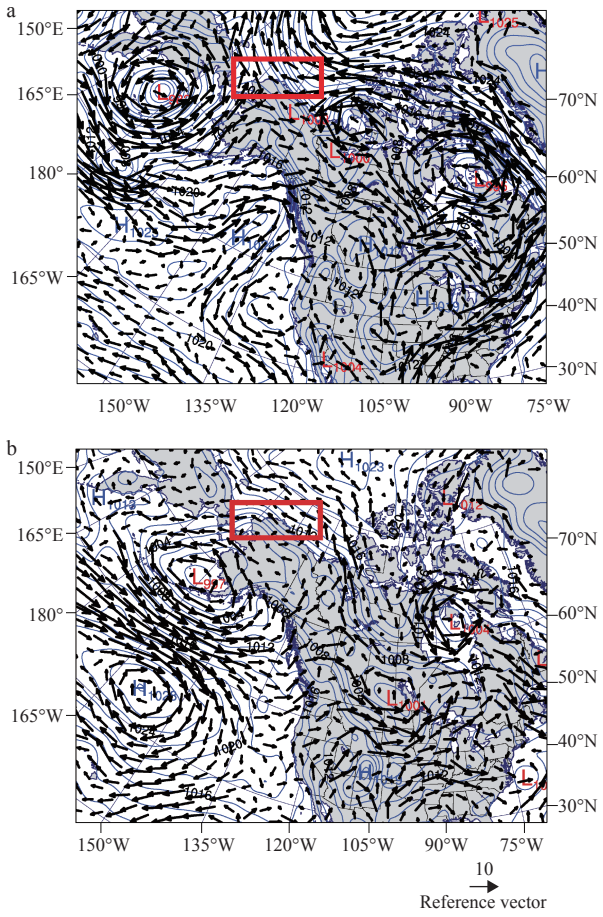

Fig. 13. Weather maps of 00:00 UTC July 8 (a), and 00:00 UTC July 13, 2017. The red box shows our study area (b).

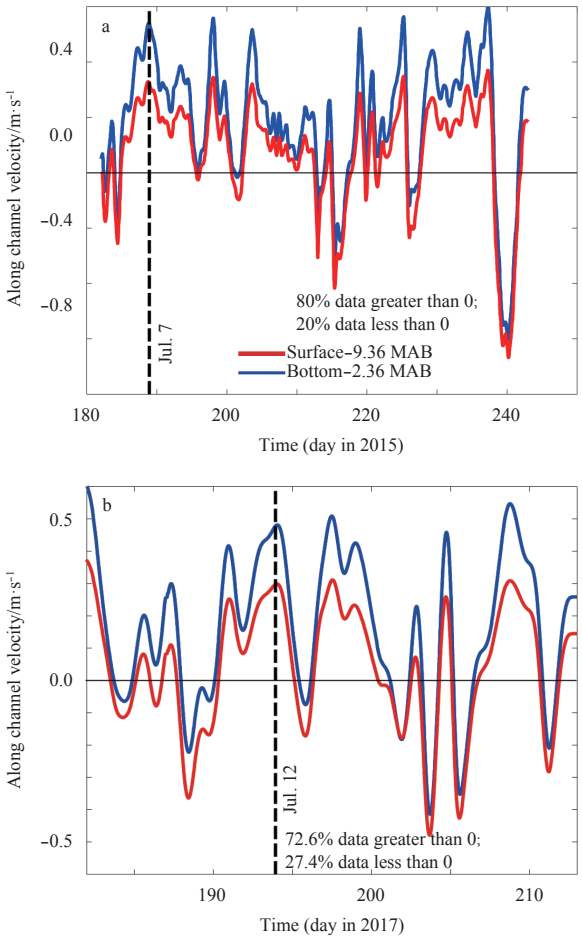

Fig. 14. Predicted surface and bottom along channel flow (m/s) for the month of July and August in 2015 (a) and July in 2017 (b) using the regression of Table 1 and wind data from Barrow Airport.

seen from the satellite image that floating ice was edging into the lagoon (Figs 12d and f).

To further verify that the regression model results are also consistent with the satellite images and weather maps, we apply the regression coefficients for equation (26) as shown in Table 1 and use the weather data from the Barrow Airport for July-Aug. 2015 and July 2017 and calculate the near surface and near bottom along channel flows. The low-pass filtered wind components (rotated to have the along channel and cross channel components) are used in the calculation. It is found that (Fig. 14a, b) during most of the three-month period, it has outward flow through the Eluitkak Pass including at the times of the Landsat observations (July 7, 2015 and July 12, 2017). This also demonstrates the practical value of the along channel flow regression with the wind data. It is interesting to note that the results (Fig. 14) show that in about 73-80% of the time there is an outward flow of water from the Elson Lagoon to the coastal ocean from the narrow Eluitkak Pass. The strong inward flow around August 27, 2015 (Fig. 14) corresponds to the time of a severe storm with northwesterly winds.

5.2 *Atmospheric frontal events*

The wind events driving the circulation and exchange flows in the Elson Lagoon are originated from synoptic scale atmospheric (high- and low-pressure) systems. The strong winds usually occur at the cold fronts separating the high-pressure systems of different air masses. The effect of frontal passages on the coastal and estuarine flows as well as related sediment transport in lower latitude regions have been more rigorously studied (e.g., Roberts et al., 1989; Walker and Hammack, 2000; Feng and Li, 2010; Li and Chen, 2014; Huang and Li, 2017; Weeks et al., 2018). As an example, Li et al. (2018b) analyzed the exchange flows through a tidal channel driven by seventy-six atmospheric fronts and concluded that the fronts provided the most significant forcing to the exchange flows with the coastal ocean. The present study provides strong evidence of similar impact of atmospheric fronts to the coastal ocean and estuaries in the high latitude arctic region. The importance of the studies on the impact to the coastal waters under such weather systems is mainly because of the repeated influence (at 3–7 d intervals) and the large scale of the weather system (~2 000–3 000 km, Li et al., 2018b). The repeated weather forcing drives the hydrodynamics and coastal erosion and sediment transport. The effect integrated over time and space will be the forcing behind the long-term impact to geomorphology, whether there is a significant climate change or not, because synoptic scale weather events are common.

5.3 *Summary*

In this paper, we have studied the wind-driven exchange flows in a lagoon with multiple inlets in the Arctic Elson Lagoon. Analysis is done to *in situ* data collected with a bottom mounted

ADCP at the Eluitkak Pass of Elson Lagoon between Beaufort and Chukchi Seas in the summer of 2013. A regression analysis is conducted using the wind velocity components and the low-pass filtered subtidal velocity at various depths, after taking out the effect of the atmospheric pressure changes as a function of time. The multi-variable correlation has the basis in physics shown by the momentum equations. The regression has high R^2 values reaching up to 0.96. We find a strong counter-wind current at the Eluitkak Pass and provide an explanation considering the wind induced torque based on the observations which are corroborated by numerical model experiments. The asymmetric inlets work together to "amplify" the wind effect: the wider eastern inlets tend to have flows in the direction of wind while the narrow Eluitkak Pass develops counter-wind flows with a significant magnitude due to the constriction. As the flow has to go through the narrow inlet, it has a strong signal correlating with the wind stress (the amplification effect). More specifically, for example, when there is northeasterly wind, the subtidal (low-pass filtered) current at the pass moves against the wind, flowing out of the Elson Lagoon through the Eluitkak Pass. The high R^2 value of the regression allows a statistical prediction of wind-induced exchange flows between the Elson Lagoon and the coastal ocean through the Eluitkak Pass, given the wind vector time series (whether from weather model prediction, hindcast, or direct measurements). The calculated currents from the regression model can then be used for applications for various purposes such as larva transport or interpretation for fishery and ecological studies. As shown by the satellite images under northeasterly and easterly wind conditions, and verified by the regression predictions for July 7 , 2015 and July 12, 2017, the lagoon system with asymmetric inlets can have strong counter-wind flows through the deeper and narrower inlet. From the regression, it is estimated that during 73%–80% of the time there was an outward flow from the Elson Lagoon to the coastal ocean through the narrow Eluitkak Pass in July and August of 2015 and July 2017.

The flow through the narrow and deep northwestern inlet is consistent with the continuity requirement such that significant counter-wind current must develop for mass balance. The wind-stress applied to a system with differences in depth or width among different inlets can produce a torque that generates the circulation pattern we have discussed (flow is downwind in shallower water or wider inlet and against the wind in deeper or narrower inlet), which is consistent with the prismatic model of Engelund (1986). It is quite remarkable that the numerical model results for the water level difference can be captured by a simple one-dimensional quasi-steady state momentum balance between wind stress and surface slope induced pressure gradient force. In the Elson Lagoon, it appears that this is particularly true for the cross-lagoon momentum balance. This further confirms the findings in other micro-tidal systems (Huang and Li, 2017). Apparently, the atmospheric high- and low-pressure systems and associated cold fronts play important roles in providing the wind forcing, which drives the flows through the multiple inlet lagoon system. In contrast, the tidally-driven flows are much less important, at subtidal scales.

Acknowledgements

Supports at all scales by and discussion with Mark Barton, Joanna Vollenweider, Ron Heintz, Brenda Norcross, Leandra Sousa and others are highly appreciated. Without these collaborative activities, this work would not have been possible. Logistic support was provided by both the North Slope Borough and UMIAQ. Review comments from two anonymous reviewers helped the improvement of the manuscript. This is contribution #116 from the Center for Coastal Oceans Research in the Institute of Water and Environment at Florida International University.

References

Aubrey D G, Giese G S. 1993. Formation and Evolution of Multiple Tidal Inlets. Washington: AGU

Brumbaugh R D. 1996. Recruitment of blue crab, Callinectes sapidus, postlarvae to the back-barrier lagoons of Virginia's eastern shore [dissertation]. Norfolk, Virginia: Old Dominion University, 174

Casares-Salazar R, Mariño-Tapia I. 2016. Influence of the remote forcing and local winds on the barotropic hydrodynamics of an elongated coastal lagoon. Journal of Coastal Research, 32(1): 116–130

Duran-Matute M, Gerkema T, Sassi M G. 2016. Quantifying the residual volume transport through a multiple-inlet system in response to wind forcing: The case of the western Dutch Wadden Sea. Journal of Geophysical Research: Oceans, 121(12): 8888–8903, doi: 10.1002/jgrc.v121.12

Emery W J, Thomson R E. 2004. Data Analysis Methods in Physical Oceanography. 2nd ed. Amsterdam: Elsevier, 654

Engelund F. 1986. Steady wind set-up in prismatic lakes. In: Pedersen F B, ed. Environmental Hydraulics: Stratified Flows. Berlin, Heidelberg: Springer-Verlag, 205–212

Feng Zhixuan, Li Chunyan. 2010. Cold-front-induced flushing of the Louisiana Bays. Journal of Marine Systems, 82(4): 252–264, doi: 10.1016/j.jmarsys.2010.05.015

Fischer H B. 1976. Mixing and dispersion in estuaries. Annual Review of Fluid Mechanics, 8: 107–133, doi: 10.1146/annurev.fl.08.010176.000543

Gibbs M, Abell J, Hamilton D. 2016. Wind forced circulation and sediment disturbance in a temperate lake. New Zealand Journal of Marine and Freshwater Research, 50(2): 209–227, doi: 10.1080/00288330.2015.1116998

Haralampides K. 2000. A study of the hydrodynamics and salinity regimes of the Lake Pontchartrain system [dissertation]. New Orleans: University of New Orleans, 219

Herrling G, Winter C. 2015. Tidally- and wind-driven residual circulation at the multiple-inlet system East Frisian Wadden Sea. Continental Shelf Research, 106: 45–59, doi: 10.1016/j.csr.2015.06.001

Huang Wei, Li Chunyan. 2017. Cold front driven flows through multiple inlets of Lake Pontchartrain estuary. Journal of Geophysical Research: Oceans, 122(11): 8627–8645, doi: 10.1002/2017JC012977

Huang Wenrui, Sun H, Nnaji S, et al. 2002. Tidal hydrodynamics in a multiple-inlet estuary: Apalachicola Bay, Florida. Journal of Coastal Research, 18(4): 674–684

Janzen C D, Wong K C. 1998. On the low-frequency transport processes in a shallow coastal lagoon. Estuaries, 21(4): 754–766, doi: 10.2307/1353279

Kjerfve B. 1986. Comparative oceanography of coastal lagoons. In: Wolfe D A, ed. Estuarine Variability. New York: Academic Press, 63–81

Kjerfve B, Magill K E. 1989. Geographic and hydrodynamic characteristics of shallow coastal lagoons. Marine Geology, 88(3–4): 187–199

Li Chunyan. 2013. Subtidal water flux through a multi-inlet system: observations before and during a cold front event and numerical experiments. Journal of Geophysical Research: Oceans, 118(4): 1877–1892, doi: 10.1002/jgrc.20149

Li Chunyan, Chen Changsheng. 2014. Shelf circulation prior to and post a cold front event measured from vessel-based acoustic Doppler current profiler. Journal of Marine Systems, 139: 38–50, doi: 10.1016/j.jmarsys.2014.05.006

Li Chunyan, Huang Wei, Chen Changsheng, et al. 2018a. Flow regimes and adjustment to wind-driven motions in Lake Pontchartrain estuary: a modeling experiment using FVCOM.

Journal of Geophysical Research: Oceans, 123(11): 8460–8488, doi: 10.1029/2018JC013985

Li Chunyan, Weeks Eddie, Huang Wei, et al. 2018b. Weather-induced transport through a tidal channel calibrated by an unmanned boat. Journal of Atmospheric and Oceanic Technology, 35(2): 261–279, doi: 10.1175/JTECH-D-17-0130.1

Li Chunyan, Weeks E, Rego J L. 2009. In situ measurements of saltwater flux through tidal passes of Lake Pontchartrain estuary by Hurricanes Gustav and Ike in September 2008. Geophysical Research Letters, 36(19): L19609, doi: 10.1029/2009GL039802

Li Chunyan, Wei Huang, Brian Milan. 2019. Atmospheric cold front induced exchange flows through a microtidal multi-inlet Bay: analysis using Multiple Horizontal ADCPs and FVCOM simulations. Journal of Atmospheric and Oceanic Technology, doi: 10.1175/JTECH-D-18-0143.1

Lin Jun, Li Chunyan, Boswell K M, et al. 2016. Examination of winter circulation in a northern Gulf of Mexico estuary. Estuaries and Coasts, 39(4): 879–899, doi: 10.1007/s12237-015-0048-y

Okkonen S R. 2008. Exchange between Elson Lagoon and the Nearshore Beaufort sea and its role in the aggregation of zooplankton. US Minerals Management Service, Outer Continental Shelf Study, vol 1008-010

Pacheco A, Ferreira Ó, Williams J J, et al. 2010. Hydrodynamics and equilibrium of a multiple-inlet system. Marine Geology, 274(1–4): 32–42, doi: 10.1016/j.margeo.2010.03.003

Parker B B. 1984, Frictional effects on the tidal dynamics of shallow estuary [dissertation]. Baltimore MD: Johns Hopkins University, 291

Pritchard D W. 1956. The dynamic structure of a coastal plain estuary. Journal of Marine Research, 15: 33–42

Proudman J. 1953. Dynamical Oceanography. London: Wiley, 409

Roberts H H, Huh O K, Hsu S A, et al. 1989. Winter storm impacts on the Chenier Plain Coast of Southwestern Louisiana. Gulf Coast Association of Geological Societies Transactions, 39: 515–522

Serreze M C, Carse F, Barry R G. 1997. Icelandic low cyclone activity: climatological features, linkages with the NAO, and relationships with recent changes in the northern hemisphere circulation. Journal of Climate, 10(3): 453–464, doi: 10.1175/1520-0442(1997)010<0453:ILCACF>2.0.CO;2

van de Kreeke J. 1985a. Stability of multiple inlets. In: Proceedings of the 19th International Conference on Coastal Engineering. Houston, Texas: American Society of Civil Engineers, 1360–1370

van de Kreeke J. 1985b. Stability of tidal inlets—Pass Cavallo, Texas. Estuarine, Coastal and Shelf Science, 21(1): 33–34, doi: 10.1016/0272-7714(85)90004-6

van de Kreeke J. 1990. Can multiple tidal inlets be stable? Estuarine, Coastal and Shelf Science, 30(3): 261–273, doi: 10.1016/0272-7714(90)90051-R

Vavrus S J. 2013. Extreme Arctic cyclones in CMIP5 historical simulations. Geophysical Research Letters, 40(23): 6208–6212, doi: 10.1002/2013GL058161

Umgiesser G, Ferrarin C, Cucco A, et al. 2014. Comparative hydrodynamics of 10 Mediterranean lagoons by means of numerical modeling. Journal of Geophysical Research: Oceans, 119(4): 2212–2226, doi: 10.1002/2013JC009512

Walker N D, Hammack A B. 2000. Impacts of winter storms on circulation and sediment transport: Atchafalaya-vermilion Bay Region, Louisiana, U.S.A. Journal of Coastal Research, 16(4): 996–1010

Weeks E, Robinson M E, Li Chunyan. 2018. Quantifying cold front induced water transport of a bay with *in situ* observations using manned and unmanned boats. Acta Oceanologica Sinica, 37(11): 1–7, doi: 10.1007/s13131-018-1330-1

Westerink J J, Luettich R A Jr, Scheffner N W. 1993. ADCIRC: An advanced three dimensional circulation model for shelves coasts and estuaries. Report 3: Development of a tidal constituent data base for the Western North Atlantic and Gulf of Mexico. Dredging Research Program Technical Report DRP-92-6. Vicksburg: US Army Engineers Waterways Experiment Station

Wu Qigang, Zhang Jing, Zhang Xiandong, et al. 2014. Interannual variability and long-term changes of atmospheric circulation over the Chukchi and Beaufort Seas. Journal of Climate, 27(13): 4871–4889, doi: 10.1175/JCLI-D-13-00610.1

Zhang Xiangdong, Walsh J E, Zhang Jing, et al. 2004. Climatology and interannual variability of Arctic cyclone activity: 1948–2002. Journal of Climate, 17(12): 2300–2317, doi: 10.1175/1520-0442(2004)017<2300:CAIVOA>2.0.CO;2